# Interaction of elastic bodies via surface forces
# 2. Exponential decay

Olga I. Vinogradova [a,b,*] and François Feuillebois [c]

[a] *Max Planck Institute for Polymer Research, Ackermannweg 10, 55128 Mainz, Germany*
[b] *Laboratory of Physical Chemistry of Modified Surfaces, Institute of Physical Chemistry, Russian Academy of Sciences,*
*31 Leninsky Prospect, 117991 Moscow, Russia*
[c] *Laboratoire de Physique et Mécanique des Milieux Hétérogènes, ESPCI, 10 rue Vauquelin,*
*75231 Paris Cedex 05, France*

## Abstract

Our goal is to study theoretically the effect of deformation on the exponentially decaying interaction of two elastic solids separated by a thin liquid film. The deformed shape of the surfaces and the contribution of the elasticity to the total force, i.e., an additional term present between elastic bodies, are calculated from continuum elastic theory via a new asymptotic technique. Both the deformation and the contribution of the elasticity to the force are found to be significant on the length scale over which the surface force acts. The surface deformation is exponentially decaying with a decay length equal to that of the original surface interaction. It is especially important for large and/or rapidly changing force. The contribution of the elasticity is also exponentially decaying, but with half the decay length. Its strength depends on the elastic constants and size of the solids and on the magnitude and gradient of the original surface force. Depending on how the separation is detected, it can appear either as an attractive or as a repulsive contribution to the force. Our results open the possibility of recalculating the measured force to the interaction free energy.

## 1. Introduction

Most theoretical and experimental studies of surface forces, or the forces acting between microscopic or even macroscopic bodies when they are in close proximity, have been conducted assuming that the surfaces are rigid [1]. However, the solids are usually elastic. Therefore, they can be deformed during the interaction. While the elastic distortion of solids at contact (adhesion) has been intensively studied by invoking either infinitely short-range [2–5] or finite-range [6–8] surface forces, precontact deformation is not predicted by classical theories and has attracted much less attention, although there are some theoretical results for repulsive interactions [9,10], as well as some numerical calculations [11].

In the previous paper [12], we adopted simplifying approximations, which led to explicit asymptotic formulas for deformation caused by power-law attractive forces. The asymptotic expressions for deformation have been used to calculate analytically the interaction force between elastic bodies and to demonstrate that it differs dramatically from the force in the case of rigid surfaces. The main point of this, the second paper, will be to extend this approach to the case of exponentially decaying interaction. This type of interaction represents both the repulsive (double-layer [13,14] and hydration [15]) and the attractive (hydrophobic [16–18]) forces, and is therefore important for understanding various phenomena, such as adhesion, cavitation, and colloidal stability. The current work is concerned only with deformation away from contact, or precontact deformation, and gives a simple but accurate description of the exponentially decaying interaction of elastic surfaces.

Our paper is arranged as follows: In Section 2 we present a brief description of the main experimental techniques. The system and approach are defined in Section 3, and the asymptotic solution for deformation is given in Section 4. The results of our calculations of interaction forces between elas-

* Corresponding author.
    *E-mail address:* vinograd@mpip-mainz.mpg.de (O.I. Vinogradova).

tic bodies are presented in Section 5. We conclude in Section 6.

## 2. Force measurement technique

As before [12], we will examine two main experimental devices, the surface force apparatus (SFA) and the atomic force microscope (AFM). We will also consider a third method, the so-called measurement and analysis of surface interaction and forces (MASIF) technique.

The SFA [19] uses mica surfaces, with a radius of curvature $R \sim 1$–$2$ cm, glued to polished silica discs with an epoxy resin. One surface is mounted at the end of a double-cantilever force measuring spring. The surface separation is determined by multiple-beam interferometry, which also allows surface deformation to be monitored in situ.

The AFM [20] uses so-called colloid probes of $R \sim 1.5$–$5$ µm, glued or melted to the end of a single microfabricated cantilever. In the case of rigid bodies the absolute separation is inferred from the deflection vs piezo position behavior, and the contact is assumed to take place at "constant compliance," i.e., when the deflection of the cantilever becomes linear with respect to sample displacement. The main difficulty with AFM measurements on deformable systems is that there is no sharp transition between contact and non-contact because deformation occurs prior to contact. This means that the zero of separation cannot be determined in the same ways as for rigid bodies. However, several methods have been used in attempts to resolve the problem for some special cases [21–25].

In the MASIF [26] spherical surfaces ($R \sim 1$ mm) are mounted at the end of a piezoelectric bimorph, which permits the spring bending to be measured electronically. The surface separation can then be calculated from this bending as in the AFM.

## 3. Analysis

### 3.1. Model

We consider two smooth elastic spheres with radii $R_1$ and $R_2$, and a situation in which the gap between the spheres is small compared to the smaller of their radii. In this approximation, the interaction of two spheres (AFM, MASIF) is equivalent to the interaction of a sphere with a plane (AFM), which is in turn the same as for two crossed cylinders of equal radii (SFA) [27–30]. The deformed and undeformed surfaces of the two spheres are sketched in Fig. 1. The undeformed spherical surface $\tilde{H}$ can be approximated by a paraboloid,

$$\tilde{H}(r) = h + \frac{r^2}{2R}, \tag{1}$$

where $R$ is the reduced radius $R_1 R_2 / (R_1 + R_2)$, and $h$ is the distance between the undeformed spheres. Here and below
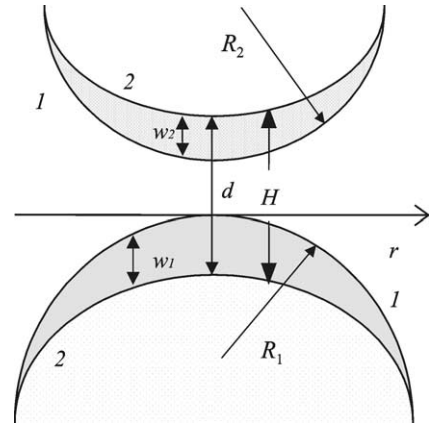


Fig. 1. Schematic of the deformation of two elastic spheres separated by a thin film. Curves 1 and 2 denote the undeformed surfaces and the actual deformed surfaces, respectively.

we focus only on the precontact situation, so that $h$ is assumed to be positive. The deformed gap profile can be given locally as

$$H(r) = \tilde{H}(r) + w(r), \tag{2}$$

where $w(r) = w_1(r) + w_2(r)$ is the sum of the deformations of the two surfaces from their original shape. A deformation toward the opposing surfaces is defined as negative, and one away from it as positive.

In order to determine the deformation we shall follow the ideas of the Hertz contact theory of linear elasticity [31] and also the developments in [6,9,12,32,33], whose authors studied deformation due to the action of surface and hydrodynamic forces. The normal displacement of the surface at a point $r$ off the central axis under a given disjoining pressure $\Pi(r)$ is [32,33]

$$w(r) = \frac{4\theta}{\pi} \int_0^\infty \Pi(y) \phi(r, y) \, dy, \tag{3}$$

where the parameter $\theta$ in (3) is defined as

$$\theta = \frac{1 - v_1^2}{E_1} + \frac{1 - v_2^2}{E_2}, \tag{4}$$

$v_{1,2}$ is Poisson's ratio, and $E_{1,2}$ are Young's modulus of elasticity for spheres 1, 2. The Green's function kernel is given by

$$\phi(r, y) = \frac{y}{y + r} K\left[\frac{4ry}{(r + y)^2}\right], \tag{5}$$

where $K$ is the complete elliptic integral of the first kind. The function $\phi(r, y)$ is in reality a function $\psi$ of a single variable $Z = y/r$.

## 3.2. Interaction forces

The exponentially decaying pressure between undeformed surfaces $\tilde{\Pi}_e$ can be described as

$$\tilde{\Pi}_e(\tilde{H}) = \frac{B}{2\pi\lambda} \exp\left(-\frac{\tilde{H}}{\lambda}\right), \tag{6}$$

with the coefficient $B$ and the decay length $\lambda$. This pressure corresponds to an electrostatic (repulsive) component of the DLVO model [13,14]. In this case $B = 4\pi\epsilon\epsilon_0\psi_0^2/\lambda$, where $\epsilon\epsilon_0$ is the dielectric constant, $\psi_0$ is the surface potential, and $\lambda$ is equal to the Debye screening length $\kappa^{-1}$. Hydration forces [15] can also be a model with a single exponential decay with much shorter $\lambda$ and positive $B$. Finally, the hydrophobic attractive force can in general be modeled as a single [17,18,34,35] or a double exponential function [16]. In this case, for the longer range part $B$ is on the order of $-10^{-3}$ N/m, and $\lambda$ can be as large as 30 nm. For the shorter range part $B$ is roughly $-0.5$ N/m and $\lambda = 1$ nm.

For rigid solids, the interaction force $\tilde{F}(h)$ is connected with the interaction free energy $\tilde{E}(h)$ between two planar half-spaces by the Derjaguin approximation [27,28]:

$$\tilde{F}(h) = 2\pi R \times \tilde{E}(h). \tag{7}$$

Interaction free energy is a universal quantity characteristic of the surfaces and the fluid, which, according to (7), can be derived from the measurements of the forces between rigid bodies:

$$\tilde{F}(h) = 2\pi R \int_h^\infty \tilde{\Pi}(\tilde{H})\,d\tilde{H} = BR \exp\left(-\frac{h}{\lambda}\right). \tag{8}$$

When the measurements deviate from theory, an extra force is inferred to be present.

Mathematically, the derivation of the Derjaguin approximation (7) uses the possibility of expressing $\tilde{\Pi}(r)$ as $\tilde{\Pi}(\tilde{H}(r))$.

## 3.3. Elastic constants

The effective elastic constants of the mica–glue system may be easily calculated from the radius of the contact zone and the pull-off force measured in the SFA [36,37]. The measured values of the elastic constants, recalculated to $\theta$, are large, on the same order as that of silica, $\theta = 1.9 \times 10^{-11}$ m²/N, and only a factor 3 or 4 less than that of mica, $\theta = 6.7 \times 10^{-12}$ m²/N. The average of all the measurements [38] is $(3.2 \pm 1.3) \times 10^{-11}$ m²/N. The recent development of the reflection SFA technique [39], however, makes it possible to work with much softer surfaces. The MASIF and AFM experiments have already been performed with soft materials, such as, for example, solid polymers [25,35]. In this case $\theta$ can be as large as $5.5 \times 10^{-10}$ m²/N.

## 4. Asymptotic solution

### 4.1. Deformation profile

The solution of the system of equations (2) and (3) and the equation describing pressure between the surfaces for $H$ and $w$ in general requires a numerical method. However, for small deformation ($w \ll h$), these equations can be solved by an asymptotic method. In this case, in the first approximation the deformation can be determined via the pressure profile in the absence of deformation $\tilde{\Pi}(\tilde{H})$ [32,33]. Strictly speaking, our problem has two characteristic length scales, $h$ and $\lambda$, so that some additional restrictions can be imposed.

In this case, putting (6) into (3), we get

$$w_e(r) = \pm\frac{2}{\pi^2} \frac{\Lambda^{3/2}}{\lambda^{1/2}} \exp\left(-\frac{h}{\lambda}\right) J_e(X), \tag{9}$$

where we define the normalized distance from the axis,

$$X = \frac{r}{\sqrt{R\lambda}},$$

the deformation length,

$$\Lambda = \theta^{2/3}|B|^{2/3}R^{1/3},$$

and the integral,

$$J_e(X) = \int_0^\infty \exp\left(-\frac{Y^2}{2}\right) \psi\left(\frac{Y}{X}\right) dY. \tag{10}$$

In Eq. (9), the plus sign holds for a repulsive force ($B > 0$), and the minus sign for an attractive force ($B < 0$). Here, we also made the following change of variable in (3):

$$Y = \frac{y}{\sqrt{R\lambda}}.$$

Already from Eq. (9) it follows that deformation decays exponentially with separation, and that the decay length is equal to that of the surface force that caused it.

Following [9], it happens that in the particular case of an exponential force, the integral (10) may be written in closed form (see their Eq. (A2.5)) as

$$J_e = \frac{\pi^{3/2}2^{1/2}}{4} \exp\left(-\frac{X^2}{4}\right) I_0\left(-\frac{X^2}{4}\right), \tag{11}$$

where $I_0$ is the Bessel function. For another type of force, the integral giving the deformation must be in general calculated numerically. We performed this calculation as a check of the above formula. Since $\psi(Z)$ has a logarithmic singularity in $Z = 1$, viz.,

$$\psi(Z) \sim \frac{1}{2} \log\left(\frac{8}{|Z-1|}\right), \tag{12}$$

we first write $J_e$ in two parts as in Eq. (A.3) in Appendix A, then extract the singularity using (12) in each integral and integrate the singular contributions by parts. Results are plotted in Fig. 2.
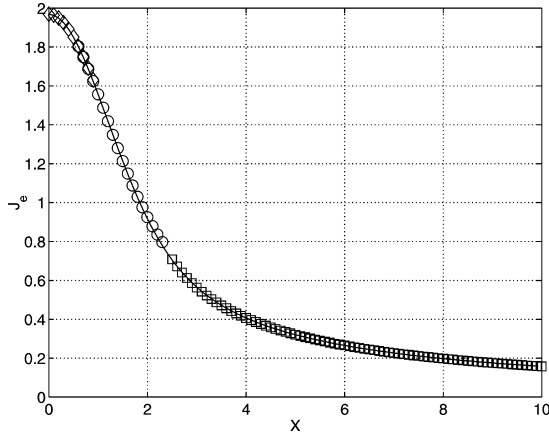
Fig. 2. Results for $J_e$ as a function of $X$. Exact results (solid curve) and various approximations: Padé approximant around $X = 2$ (circles), peak approximation (diamonds) for smaller $X$, and tail approximation (squares) for larger $X$. The various approximations appear here superimposed onto the exact results (the maximum difference being $2.5 \times 10^{-3}$).

For practical purposes, it is also useful to obtain approximation formulae. Analytic expansions may be obtained in the limits of small and large $X$.

### 4.1.1. Small distances from the axis, or "peak"

For small normalized distances $X$, we calculate the expansion from (11):

$$J_{e,\text{peak}}(X) = \frac{\sqrt{2}\pi^{3/2}}{4}\left(1 - \frac{1}{4}X^2 + \frac{3}{64}X^4 + O(X^6)\right).$$

For another type of force for which no closed form such as (11) exists, such an expansion can be calculated as shown in Appendix A, in which the above expansion is checked. All terms are even, as could be anticipated from symmetry; the deformation profile is, to this order,

$$w_{e,\text{peak}}(X) = \pm\frac{1}{\sqrt{2\pi}}\frac{\Lambda^{3/2}}{\lambda^{1/2}}$$
$$\times \exp\left(-\frac{h}{\lambda}\right)\left(1 - \frac{1}{4}X^2 + \frac{3}{64}X^4\right).$$

From the numerical calculations of $J_e(X)$, the maximum deformation is found to be on the axis, so that its value is

$$w_{e,\text{max}} = \pm\frac{1}{\sqrt{2\pi}}\frac{\Lambda^{3/2}}{\lambda^{1/2}}\exp\left(-\frac{h}{\lambda}\right),$$

and the actual distance at the point of closest approach is then

$$d = h \pm \frac{1}{\sqrt{2\pi}}\frac{\Lambda^{3/2}}{\lambda^{1/2}}\exp\left(-\frac{h}{\lambda}\right). \tag{13}$$

Equation (13) demonstrates that at separation $h$ such that $\lambda \ll h$, the change in surface separation, $\delta d$, is equal to how far surfaces have been moved, $\delta h$. When surfaces are in close proximity, $h \sim \lambda$ or $h \ll \lambda$, this is no longer the case. For an attractive interaction (when the minus sign holds) the surfaces are pulled toward each other, and $d$ decreases more
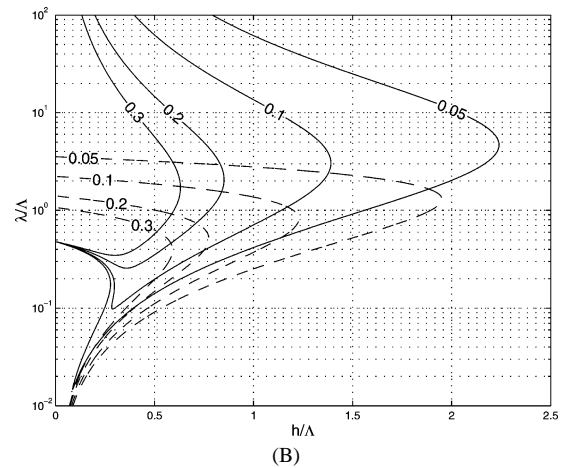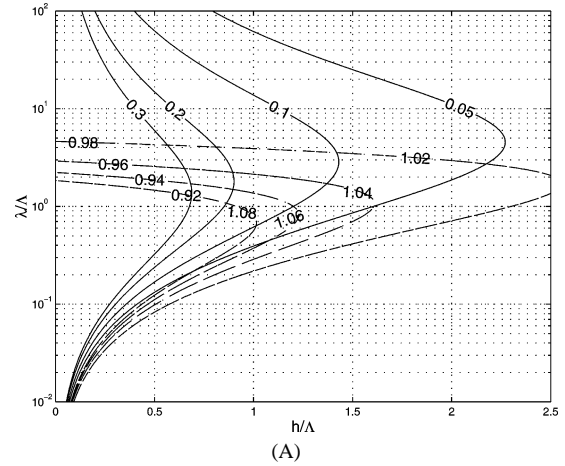




Fig. 3. (A) Solid lines: isolines of the function $|w_{e,\text{max}}/h|$ in the first order approximation. Dashed lines: isolines of the normalized curvature $R/R_{\text{eff}}$, Eq. (15); there is a superposition of the sets of lines $R/R_{\text{eff}} < 1$ for a repulsive force and $> 1$ for an attractive force. (B) Solid lines: isolines of the function $|w_{e,\text{max}}/h|$ in the second order approximation, that is, $|(d-h)/h|$ from Eq. (B.1). Dashed lines: isovalues of the ratio of the second order term to the first order term in the expression for $|w_{e,\text{max}}/h|$.

rapidly than $h$. For a repulsive interaction (when the plus sign holds) the surface separation $d$ remains larger than $h$.

The assumption that leads to Eq. (13) is that the deformation $w$ is small as compared with $h$. We will now check in which conditions this is indeed true, and whether it imposes some restrictions to the value of $\lambda$. The assumption of small deformation can be written as

$$\left|\frac{w_{e,\text{max}}}{h}\right| = \frac{1}{\sqrt{2\pi}}\frac{\Lambda}{h}\left(\frac{\Lambda}{\lambda}\right)^{1/2}\exp\left(-\frac{h}{\lambda}\right) \ll 1 \tag{14}$$

in terms of the dimensionless distance $h/\Lambda$ and dimensionless decay length $\lambda/\Lambda$. The isolines of $|w_{e,\text{max}}/h|$ are presented in Fig. 3A. Strictly speaking, the domain of applicability of our solution lies on the right side of an isoline, say 0.1 for a 10% precision. However, as we will show below, in some situations the original restriction of small deformation can be relaxed.

The radius of curvature $R_{\text{eff}}$ of the peak region can be calculated analytically by collecting the terms in $r^2$ in the

expression $H = h + r^2/(2R) + w_{e,\text{peak}}$ and writing it as $H = d + r^2/(2R_{\text{eff}})$. We then obtain the normalized curvature:

$$\frac{R}{R_{\text{eff}}} \sim 1 \mp \frac{2^{1/2}}{4\pi^{1/2}} \left(\frac{\Lambda}{\lambda}\right)^{3/2} \exp\left(-\frac{h}{\lambda}\right). \tag{15}$$

This means that the deformation involves not only a change in separation, but also a considerable change in curvature, i.e., flattening (negative sign for repulsive forces) or elongation (positive sign for attractive forces). Lines of constant $R/R_{\text{eff}}$ are also plotted in Fig. 3A. One can see that at relatively small $\lambda/\Lambda$ and $h/\Lambda$, $R/R_{\text{eff}}$ varies over a large range.

### 4.1.2. Large distances from the axis, or "tail"

Expanding (11) for large $X$, or expanding $\psi$ for large $X$ in (10) and integrating, we obtain

$$J_{e,\text{tail}}(X) = \frac{\pi}{2} \left[\frac{1}{X} + \frac{1}{2X^3} + \frac{9}{8X^5} + \frac{75}{16X^7} + O\left(\frac{1}{X^9}\right)\right].$$

Therefore,

$$w_{e,\text{tail}}(X) \sim \pm \frac{1}{\pi} \frac{\Lambda^{3/2}}{\lambda^{1/2}} \exp\left(-\frac{h}{\lambda}\right)$$
$$\times \left[\frac{1}{X} + \frac{1}{2X^3} + \frac{9}{8X^5} + \frac{75}{16X^7}\right].$$

### 4.1.3. Intermediate distances from the axis, or "sloping"

For practical purposes, it is useful to have simple formulae, and we propose the expression

$$J_{e,\text{sloping}}(X)$$
$$= \frac{0.917 - 0.42(X-2) + 0.158(X-2)^2 - 0.046(X-2)^3}{1 + 0.096(X-2) + 0.0339(X-2)^2 - 0.051(X-2)^3},$$

which was obtained by expanding $J_e(X)$ as a Taylor series around $X = 2$, integrating, and then constructing a Padé approximant to improve the series convergence. Matching of this intermediate approximation with the peak approximation at $X_1 = 0.7575$ provides a $2.5 \times 10^{-3}$ precision; and matching it with the tail approximation at $X_2 = 3.214$ provides a $2 \times 10^{-3}$ precision. Decreasing the numbers of terms to 2 in the peak and tail regions and three in the intermediate region would decrease the accuracy of our description to $3.7 \times 10^{-2}$. If we keep only two terms in each region the relative accuracy is $7.7 \times 10^{-2}$. The best approximations for $J_e$ (see above formulae) are plotted together with the exact result in Fig. 2.

We remark that the first order terms of the expansion around $X = 2$ give the slope there:

$$J_{e,\text{slope}}(X) \sim 1.9322 - 0.5076X.$$

Therefore, as an approximate estimate one can use

$$w_{e,\text{sloping}}(X) \sim \pm \frac{2}{\pi^2} \frac{\Lambda^{3/2}}{\lambda^{1/2}} \exp\left(-\frac{h}{\lambda}\right)\left(2 - \frac{X}{2}\right).$$

Several main conclusions can be made from inspection of our asymptotic expressions for the deformation due to

exponentially decaying forces. First, deformation decays exponentially with separation, and its decay length is exactly the same as that of the interaction that caused it. Second, similarly to the deformation due to a power-law force [12], it is linear in $\theta$ and in the strength of interaction ($B$), and increases weakly ($\sim R^{1/2}$) with the size of interacting bodies. An important consequence would be a strong dependence of deformation due to double layer forces on the surface potential (as $B \sim \psi_0^2$). Also, much larger deformation should be expected for the SFA, due almost entirely to the large radius of curvature of the surfaces. Third, deformation depends in a complex way on $\lambda/\Lambda$ and $h/\Lambda$, and can be extremely important at relatively small values of these parameters.

### 4.2. Interaction force caused by deformation

In Ref. [33] it has been shown that in the general case it is wrong to estimate the correction to pressure (force) by assuming simply that $\Pi = \Pi(H(r))$. However, this approximation has been justified for the case of small deformation: $w \ll \tilde{H}$. If so, one can write

$$\Pi(H) = \Pi(\tilde{H} + w) = \tilde{\Pi}(\tilde{H}) + \Delta\Pi. \tag{16}$$

Substitution of the expression for exponential pressure gives

$$\Pi_e(H) = \frac{B}{2\pi\lambda} \exp\left(-\frac{\tilde{H} + w}{\lambda}\right)$$
$$= \tilde{\Pi}_e(\tilde{H}) \exp\left(-\frac{w}{\lambda}\right). \tag{17}$$

We remark and stress that $\Pi_e(H)$ is always less than $\tilde{\Pi}_e(\tilde{H})$. This means that for repulsive exponential interaction ($w > 0$) the absolute value of $\Pi_e(H)$ is also smaller than $\tilde{\Pi}_e(\tilde{H})$. An important point to note is that the resulting pressure remains positive. The new pressure tends to decrease the absolute value of deformation [41], an effect we ignore in our first-order approach. Therefore, one can conclude that the first-order approximation we develop here, being formally applied to the situation of large deformation, will overestimate it. Clearly, the opposite situation would happen in case of an attractive interaction ($w < 0$). While $\Pi(H)$ will again be less than $\tilde{\Pi}(\tilde{H})$, this will increase the absolute value of pressure [12]. The new pressure would then tend to make deformation larger, so the first-order approximation will underestimate the deformation caused by attractive forces.

As a first order approximation for the perturbation of pressure one can use $\Delta\Pi = d\tilde{\Pi}/d\tilde{H} \times w(r)$ and estimate it as

$$\Delta\Pi_e = -\frac{B \exp(-\tilde{H}/\lambda)}{2\pi\lambda^2} \times w_e(r)$$
$$= -\frac{B}{\pi^3}\left(\frac{\Lambda}{\lambda}\right)^{3/2} \exp\left(-\frac{2h}{\lambda}\right)\exp\left(-\frac{X^2}{2}\right)J_e(X). \tag{18}$$

Direct substitution of the asymptotic expressions for $J_e$ into (18) allows an estimate of $\Pi_e$ in each region and an

estimate of the second order approximation for deformation, and justifies, in some situations, the extension of the domain of applicability of the first order solution (see Appendix B).

Now we can calculate the force between elastic surfaces. In our approximation it can be presented as

$$F = 2\pi \int_0^\infty \Pi(r) r \, dr = \tilde{F}(h) + \Delta F. \tag{19}$$

Note that, with deformation, the area over which the pressure has to be integrated also changes. However, the pressure still decays fast enough so that this change of surface can be embedded in the integral for $r$ to $\infty$. Thus, the elasticity contribution caused by the exponential force can roughly be estimated as

$$\Delta F_e = 2\pi R \lambda \int_0^\infty \Delta \Pi_e(X) X \, dX$$

$$= -\frac{BR}{\lambda} \exp\left(-\frac{h}{\lambda}\right) \int_0^\infty e^{-X^2/2} w_e(X) X \, dX.$$

Thus

$$\Delta F_e = BR \left(\frac{\Lambda}{\lambda}\right)^{3/2} \exp\left(-\frac{2h}{\lambda}\right) \Omega_1,$$

where

$$\Omega_1 = \frac{2}{\pi^2} \int_0^\infty \int_0^\infty \exp\left(-\frac{X^2 + Y^2}{2}\right) \psi(X/Y) X \, dX \, dY.$$

The integral $\Omega_1$ is more easily calculated using polar coordinates $(\rho, \theta)$ in the $(X, Y)$ plane:

$$\Omega_1 = \frac{2}{\pi^2} \int_0^\infty e^{-\rho^2/2} \rho^2 \, d\rho \int_0^{\pi/2} \psi(\tan \vartheta) \cos \vartheta \, d\vartheta$$

$$= -\frac{2\sqrt{\pi/2} \times 1.11407}{\pi^2} = -0.28209.$$

(The second integral has only a weak log singularity in $\vartheta = \pi/4$.) Finally, the force is

$$F_e = \tilde{F}_e(h) + \Omega_1 BR \left(\frac{\Lambda}{\lambda}\right)^{3/2} \exp\left(-\frac{2h}{\lambda}\right)$$

$$= \tilde{F}_e(h) \left[1 + \Omega_1 \left(\frac{\Lambda}{\lambda}\right)^{3/2} \exp\left(-\frac{h}{\lambda}\right)\right]. \tag{20}$$

All the techniques for force measurement measure the real force, i.e., the force distorted by deformation and described by Eq. (20). In the AFM and MASIF experiment the separation is not measured, being inferred from force–piezo position data [21–25]. Strictly speaking, all these methods are not generally applicable. Therefore, here we simply use the fact that the AFM/MASIF measurements are corrected for separation, so that in the ideal situation the undisturbed

distance $h$ can be deduced (provided that the zero of separation is established correctly). The same assumption was made in Ref. [11]. If so, Eq. (20) can be used to connect the force measured experimentally with $\tilde{F}_e(h)$, which reflects the interaction free energy of two surfaces separated by distance $h$. Since $\Omega_1$ is negative, one can conclude that the AFM/MASIF measurements give more attractive force than would be observed between rigid bodies. Physically, this reflects the change in separation due to deformation. In the SFA experiment it is the distorted separation $d$ which is measured, so that it would be useful to express $F_e$ via $\tilde{F}_e(d)$. Expanding (8) around $h$ we get

$$\tilde{F}_e(d) - \tilde{F}_e(h) \sim -\frac{BR}{\sqrt{2\pi}} \left(\frac{\Lambda}{\lambda}\right)^{3/2} \exp\left(-\frac{2h}{\lambda}\right).$$

Then (20) can be rewritten as

$$F_e \sim \tilde{F}_e(d) + \Omega_2 BR \left(\frac{\Lambda}{\lambda}\right)^{3/2} \exp\left(-\frac{2h}{\lambda}\right), \tag{21}$$

where $\Omega_2 = 0.1168$. The positive sign of $\Omega_2$ suggests that the force curves measured with the SFA are more repulsive than one can expect for rigid surfaces. Unfortunately, in case of the SFA experiment, it is not so easy to recalculate the measured force to the interaction free energy at $d$, because Eq. (21) contains $h$, which cannot be explicitly presented as a function of $d$. One can, however, always calculate $h$ numerically, by solving Eq. (13).

The meaning of the second term in Eq. (21) can be understood if one recognizes that $F_e$ can be expressed via $\tilde{F}_e(d)$ by substituting $\Pi(H)$ into Eq. (19) and integrating by parts, which gives

$$F_e = \tilde{F}_e(d) - \frac{BR}{\lambda} \int_0^\infty \left(\frac{\partial w}{\partial r}\right) \exp\left(-\frac{H}{\lambda}\right) dr.$$

So, physically, this term reflects the change in slope near the line-of-centers due to deformation.

Some misleading ideas about the effect of small deformations on total force may have been obtained by casual readers of the publications [7,11], where the so called "slowly varying deformation approximation" (SVDA) has been introduced. The SVDA is said to be valid when "deformation varies slowly compared to curvature" (quantities being normalized) and postulates two assumptions: $w(r) \sim w_{max}$ and $F \sim \tilde{F}(d)$. As we have shown before [33], the condition for small deformation is equivalent to that of small slope $(\partial w / \partial r \ll r/R)$. This allows one to express pressure as the function of gap profile $H$, which, mathematically, resembles the tricks used to derive the Derjaguin approximation (7). However, the resulting force is not proportional to the interaction free energy per unit area between planar walls separated by $d$ as was suggested in [11], being confined between $\tilde{F}_e(h)$ and $\tilde{F}_e(d)$. Hence, in the SVDA the second term of the expression for force described by Eq. (21) is lost, although it is neither zero nor negligible.

In summary, extra force due to deformation decays exponentially with separation, with a decay length half that of the original force. The sign of this elasticity contribution depends on how the separation is detected: it can lead to either less or more repulsive force compared with the case of rigid surfaces at $h$ or $d$ respectively. Obviously the Derjaguin approximation (7) is no longer valid for elastic surfaces, but the interaction free energy per unit area can be obtained directly with the approximation suggested here.

## 5. Discussion

In this section we give some numerical examples that illustrate the above results and conclusions. We focus mostly on double layer forces, because of their importance as a part of the DLVO potential, and because of their repulsive character. We also confine ourselves to parameters typical of a surface force experiment. The generalization of our results to other types of exponentially decaying interactions or different experimental situation would be straightforward.

### 5.1. Repulsive forces

Fig. 4 illustrates the effect of double layer forces on the real separation $d$ between the surfaces. Both the first order (Eq. (13)) and second order (Eq. (B.1)) approximations are represented. As shown above, the first order approximation also is an upper bound. It is observed in Fig. 4 that the first and second approximations become close and even practically coincide for small $B$ (small $|\psi_0|$), Fig. 4A, and large $\lambda$, Fig. 4B. For small $h$, this even occurs outside of the domain of small deformation $d \ll h$. This is an indication that the domain of validity of the first order approximation is much larger than anticipated from Fig. 3B. Details about this extension are presented in Appendix B. All these curves were computed for a typical SFA radius of curvature ($R = 1$ cm). Similar calculations for a typical AFM size ($R = 10$ μm) give negligibly small deformation and $d$ practically coincides with $h$.

The surface profiles for two elastic surfaces interacting with an exponential repulsion are shown in Fig. 5 at various surface separations. For comparison, the undeformed surface shapes are also plotted. The data are plotted in this manner so that the profiles represent the shape of the fringes which would be observed during SFA experiments. One can see that as the surfaces approach each other they begin to flatten.

Computed force curves for four different surface potentials for the deflection (SFA) method and the force feedback (MASIF) method are shown in Fig. 6. As predicted, SFA measurements are more repulsive than the interaction free energy, while the MASIF measurements are more attractive. The same calculations performed with the typical radius of the AFM colloidal probe suggest that there is practically no elastic contribution to the total force. As before [12], the
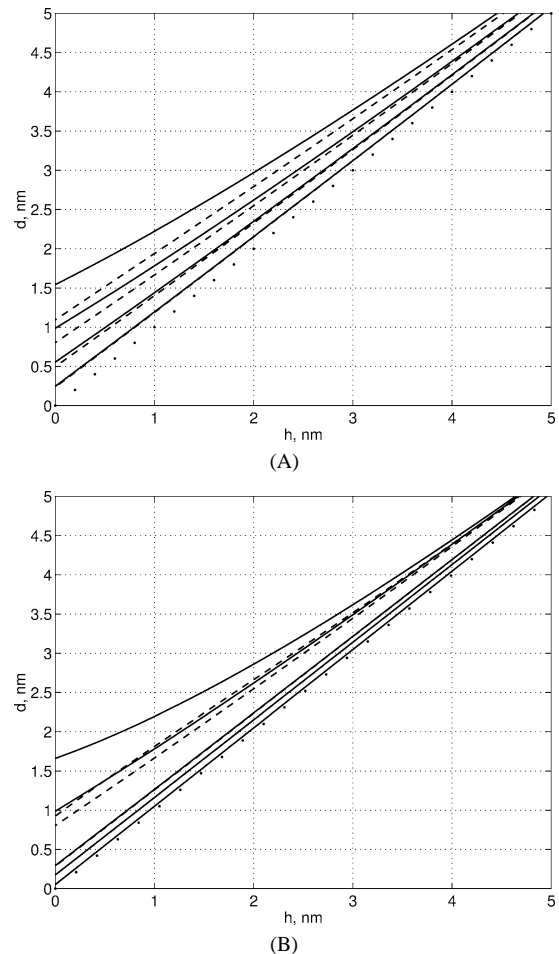


(A)

(B)

Fig. 4. A plot of the real separation $d$ between solids at the point of closest approach against the undeformed separation. In the absence of deformation $d = h$ until contact (dots). Deformation effect is due to repulsive double layer forces. Solid curves plot the first order, and dashed, the second order solution, respectively. Parameters assumed in the calculations are as follows. Effective radius $R = 1$ cm, elastic constant $\theta = 5 \times 10^{-10}$ m$^2$/N. (A) demonstrates the effect of potential, from top to bottom $|\psi_0| = 50$, 40, 30, and 20 mV, at salt concentration $5 \times 10^{-3}$ mol/L, giving a decay length of $\lambda = 4.3$ nm. (B) shows the influence of the salt concentration at $|\psi_0| = 40$ mV. From top to bottom it is $10^{-2}$, $5 \times 10^{-3}$, $10^{-3}$, $5 \times 10^{-4}$, and $10^{-4}$ mol/L, which correspond to $\lambda$ equal to 3.0, 4.3, 9.6, 13.6, and 30.4 nm.

typical SFA experiment gives more accurate results than the MASIF experiment.

Hydration forces observed between mica surfaces in aqueous electrolyte solutions [15] are of roughly exponential type and appear only at short distances. These forces are nearly independent of electrolyte type and concentration. There have previously been some arguments that surface deformation did not account for the observation of hydration forces [10], as well as arguments that the measurements of hydration forces are influenced by it [11]. The results obtained within the assumptions of our model rather support the former point of view [10]. However, we cannot exclude the possibility that for large deformation (i.e., when the effect due to change in radius will be comparable to or more
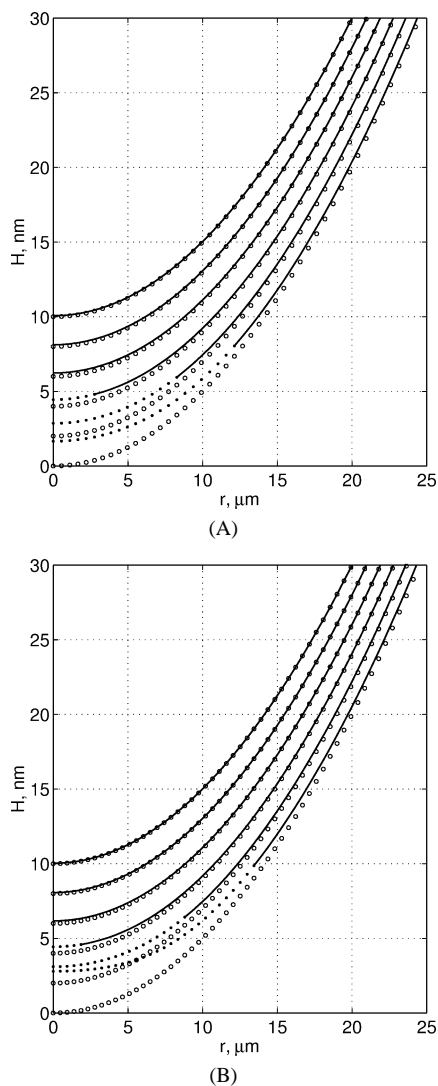
(A)



(B)

Fig. 5. Surface profiles for two surfaces interacting with a repulsive double layer force: $|\psi_0| = 40$ mV, $\theta = 5 \times 10^{-10}$ m$^2$/N, $R = 1$ cm. From top to bottom $h$ varies from 10 to 0 nm by steps of 2 nm. The circles represent the undeformed profiles. The solid lines represent the deformed profile calculated at first order for small deformation $(w/(h + r^2/(2R)) < 0.1)$. The dots represent the continuation of the preceding curves in the range where $(w/(h + r^2/(2R)) > 0.1)$. (A) $\lambda = 3.0$ nm (concentration $1 \times 10^{-2}$ mol/L); (B) $\lambda = 2.15$ nm (concentration $2 \times 10^{-2}$ mol/L).

important than the distortion of the separation), the elasticity contribution could account for most of the observed difference between DLVO theory and experiment.

### 5.2. Attractive forces

The cross-sectional surface separation for two surfaces interacting with an attractive surface force are shown in Fig. 7. The profiles are very different from those for a repulsive interaction. The computed profiles for the long-range part of the hydrophobic interaction are not disturbed by deformation. In contrast, for the short-range hydrophobic interaction we see dramatic deviations from the undeformed
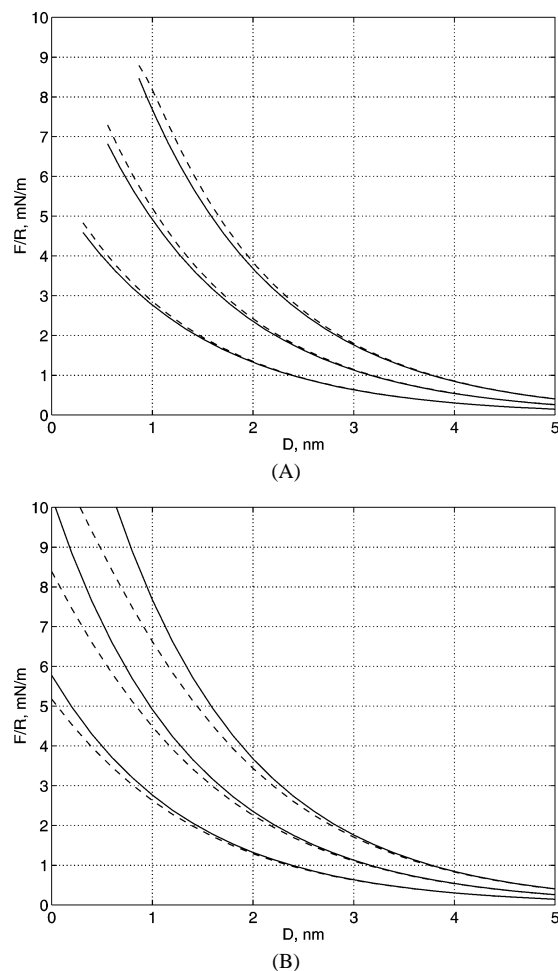


(A)



(B)

Fig. 6. Computed force curves for surfaces interacting with three different surface potentials: from top to bottom $|\psi_0| = 50$, 40, and 30 mV, $\lambda = 1.4$ nm (concentration $5 \times 10^{-2}$ mol/L). Solid curves show the force expected between the rigid bodies separated by distance $D$, dashed curves correspond to the force acting between elastic surfaces. (A) illustrates the SFA deflection method $D = d$, $R = 1$ cm, $\theta = 5 \times 10^{-11}$ m$^2$/N. (B) illustrates the MASIF feedback method $D = h$, $R = 1$ mm, $\theta = 10^{-10}$ m$^2$/N.

shapes. Shape changes are significant on the length scale over which surface forces act. This has already been discovered before for elastic solids [10] and drops [42,43] and is made evident again here in Fig. 7B.

This effect is best illustrated by the force curves shown in Fig. 8. Since the calculations performed for a long-range hydrophobic interaction do not reveal any effect of surface deformation, we consider only a situation corresponding to a short-range hydrophobic force. As expected, the deviations from the force–distance profile expected for rigid surfaces are discernible at separations considerably larger than the decay length of the force. This effect alone, however, cannot predict a long-range tail of the hydrophobic force.

All conclusions of this subsection are made by assuming that the deflection technique can be used at any separation. In other words, we have ignored the possibility of the jump instability, i.e., the fact that at some separations the direct
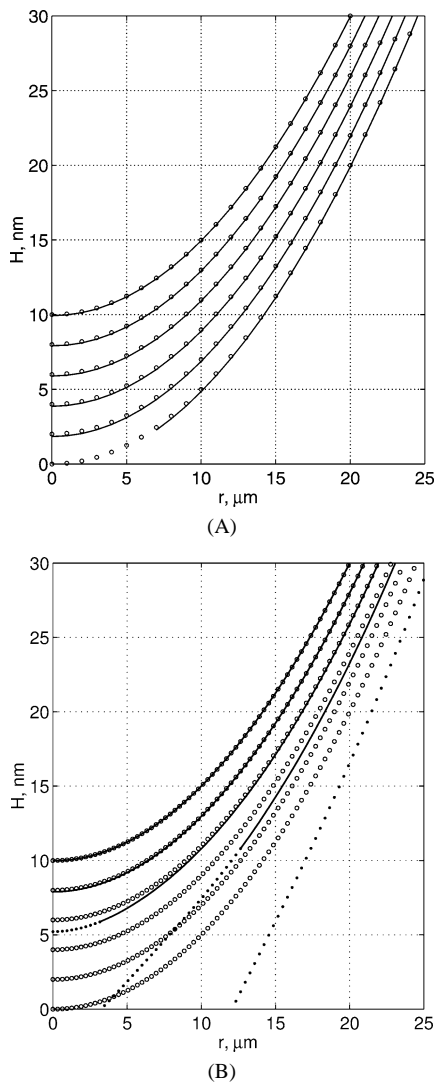
(A)



(B)

Fig. 7. Surface profiles for two surfaces interacting with an attractive force law. The circles represent the undeformed profiles. The solid lines represent the deformed profile calculated at first order for small deformation $(w/(h + r^2/(2R)) < 0.1)$. The dots represent the continuation of the preceding curves in the range where $(w/(h + r^2/(2R)) > 0.1)$. $R = 1$ cm, $\theta = 5 \times 10^{-10}$ m$^2$/N. From top to bottom $h$ varies from 10 to 4 nm by steps of 2 nm. (A) $B = -10^{-3}$ N/m, $\lambda = 10$ nm; (B) $B = -0.5$ N/m, $\lambda = 1$ nm.



Fig. 8. Computed force curves for surfaces interacting with a short range exponential force ($\lambda = 1$ nm, $B = -0.5$ N/m). The solid curve shows the force expected between rigid surfaces. Dashed curve corresponds to the SFA deflection method $D = d$, $R = 1$ cm, $\theta = 5 \times 10^{-11}$ m$^2$/N. Dots illustrate the MASIF feedback method $D = h$, $R = 1$ mm, $\theta = 10^{-10}$ m$^2$/N.

measurement of the force presented in Fig. 8 could be impossible. In the elastic system this could be mostly due to a force measuring spring [19,44] and partly due to deformation itself [5,7,45,46]. We do not address the question of a jump separation in the current paper. However, it should be stressed that our results mean that it would be wrong to extrapolate the force vs separation curve obtained by measuring the jump position to the region of short separations. In this region, the real force is more attractive then it would follow from the jump method, with dramatic consequence for adhesion and other phenomena influenced by the short-range attractive interaction forces.
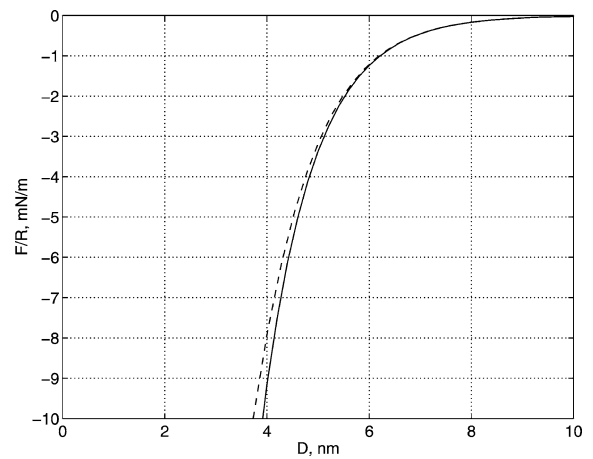
## 6. Conclusion

We have calculated analytically the shape of elastic surfaces and the total force between them as they interact through an exponentially decaying surface force, assuming that the deformation is small. The effect of elasticity is found to be especially important when the decay length of this interaction is short (rapidly changing force), and the prefactor is high (large force). The interaction force causes significant deformation which depends in a complex way on the nature of the interaction and configuration geometry, and which decays exponentially with the decay length of the original force. Deformation, in turn, produces an additional exponential force with half the decay length. All the force measurement techniques measure the total force between surfaces which includes this elasticity contribution and do not correct for error in the force due to deformation. The measured minimum separation is either real (SFA), i.e., including deformation, or corrected (AFM/MASIF). Ironically, with the same experimental parameters, the correction for separation leads to larger deviations of measured force from the force that would act between rigid surfaces (interaction free energy). This reflects the fact that when deformation is small (and/or varies slowly with slope), the change in separation due to deformation is more important than the change in radius near the line-of-centers. We believe our results provide an important tool to correct the measured force between elastic surfaces to the true interaction free energy.

## Acknowledgment

**Appendix A. Expansion of the integral in $J_e$ for small $X$**

Let us find the expansion of $J_e$, defined in (10), for small $X$. Since $\psi(Z)$ has a logarithmic singularity at $Z = 1$, we write it in two parts, one from $Y = 0$ to $X$ and one from $Y = X$ to $\infty$. Let $Z = Y/X$ in the first part and $Z = X/Y$ in the second part. Then

$$J_e(X) = X \int_0^1 \exp\left(-\frac{Z^2 X^2}{2}\right) \psi(Z)\, dZ$$

$$+ X \int_0^1 \frac{1}{Z^2} \exp\left(-\frac{X^2}{2Z^2}\right) \psi\left(\frac{1}{Z}\right) dZ. \tag{A.1}$$

Now from its definition, for $Z \neq 0$ the function $\psi$ satisfies

$$\psi\left(\frac{1}{Z}\right) = \frac{1}{Z} \psi(Z), \tag{A.2}$$

so that

$$J_e(X) = X \int_0^1 \exp\left(-\frac{Z^2 X^2}{2}\right) \psi(Z)\, dZ$$

$$+ X \int_0^1 \frac{1}{Z^3} \exp\left(-\frac{X^2}{2Z^2}\right) \psi(Z)\, dZ. \tag{A.3}$$

Let the first integral be $I$ and the second one be $J$.

*A.1. Expansion of I*

In the expression (5) providing the function $\psi$, we will use the definition of the elliptic integral $K$,

$$K(x) = \int_0^{\pi/2} \frac{d\alpha}{\sqrt{1 - x \sin^2 \alpha}},$$

so that

$$\psi(Z) = \int_0^{\pi/2} f(Z, \alpha)\, d\alpha,$$

where

$$f(Z, \alpha) = \frac{Z}{\sqrt{(Z + 1)^2 - 4Z \sin^2 \alpha}}. \tag{A.4}$$

The integral $I$ is first expanded in $X$; then each term in the expansion is first integrated analytically in $Z$ and then in $\alpha$.

*A.2. Expansion of J*

The calculation of $J$ should be treated with care since the integral becomes singular for $X \to 0$. This is a typical singular perturbation problem. The singularity is extracted by using an expansion of $\psi$ for small $Z$. We then need an expansion for $f$, Eq. (A.4), for small $X$, which is written symbolically as

$$f(Z, \alpha) = \sum_{m=1}^2 \beta_m(\alpha) Z^m + R(\alpha, Z). \tag{A.5}$$

Then

$$J = \int_0^1 \frac{1}{Z^3} \exp\left(-\frac{X^2}{2Z^2}\right) \int_0^{\pi/2} f(Z, \alpha)\, d\alpha\, dZ \tag{A.6}$$

is written as $J_r + J_s$, where

$$J_r = \int_0^{\pi/2} \int_0^1 \frac{1}{Z^3} \exp\left(-\frac{X^2}{2Z^2}\right) R(Z, \alpha)\, dZ\, d\alpha \tag{A.7}$$

is regular because of the $O(Z^3)$ behavior of $R(Z, \alpha)$, and

$$J_s = \sum_{m=1}^4 \left(\int_0^{\pi/2} \beta_m(\alpha)\, d\alpha\right) \int_0^1 z^{m-3} \exp\left(-\frac{X^2}{2Z^2}\right) dZ \tag{A.8}$$

contains the singular part.

As for $J_r$, the integral with the exponential could not be calculated analytically. But using a first order expansion of the exponential for small $X$, that is, replacing the exponential by unity, we still have a convergent integral which can be integrated analytically first in $Z$ and then in $\alpha$.

As for $J_s$, the singularity in (A.8) is resolved in the classical way, using a stretched variable $\hat{Z} = Z/X$. The integrals in $\hat{Z}$ are convergent in $\hat{Z} = 0$ because of the exponential; they can be integrated analytically.

*A.3. Result for $I_e$*

Analytical calculations give

$$I = 1 + O(X^2), \tag{A.9}$$

$$J_r = -1 + \frac{3}{8}\pi + O(X^2), \tag{A.10}$$

$$J_s = \frac{\sqrt{2}}{4X}\pi^{3/2} - \frac{3}{8}\pi - \frac{\sqrt{2}}{16}\pi^{3/2} X + O(X^2). \tag{A.11}$$

It is seen that as a result of matching, which is performed by simply adding up the parts of the integral, $J_e = X(I + J_r + J_s)$, some terms cancel out. The final result is

$$J_e \sim \frac{\sqrt{2}\pi^{3/2}}{4}\left(1 - \frac{1}{4}X^2\right). \tag{A.12}$$

To calculate higher order terms analytically, we have to be careful that expanding the exponential to higher order in (A.7) would give divergent integrals in $Z = 0$. Thus $R(Z, \alpha)$ has to be more regular in $Z = 0$. The upper value $m = 2$ in (A.5) should be replaced by a higher value $m = M$. Taking

$M = 10$, we could calculate with Maple computer algebra

$$J_e = \frac{\sqrt{2}\pi^{3/2}}{4}\left(1 - \frac{1}{4}X^2 + \frac{3}{64}X^4 - \frac{5}{768}X^6 + \frac{35}{49152}X^8\right), \tag{A.13}$$

and the next term would be $O(X^{10})$.

## Appendix B. Second order approximation for maximum deformation

We have calculated the deformation, assuming that the pressure is not disturbed. However, as we have shown, the deformation causes a change in the pressure. The calculation of the second order solution can be obtained by using Eq. (18) instead of (6) in (3). Here we only estimate the maximum deformation, that is, the amount by which the central part of the two surfaces would be displaced elastically. This is given by [40]

$$w_{\max} = 2\theta \int_0^\infty \Pi(r)\,dr$$

$$= \frac{1}{\sqrt{2\pi}}\frac{\Lambda^{3/2}}{\lambda^{1/2}}\exp\left(-\frac{h}{\lambda}\right) + 2\theta\int_0^\infty \Delta\Pi_e(r)\,dr.$$

The mathematical manipulations and calculation of the integral

$$2\theta\int_0^\infty \Delta\Pi_e(r)\,dr = -\frac{2\Lambda^3}{\pi^3\lambda^2}\exp\left(-\frac{2h}{\lambda}\right)$$
$$\times \int_0^\infty J_e(X)\exp\left(-\frac{X^2}{2}\right)dX$$

give

$$\Upsilon = \int_0^\infty J_e(X)\exp\left(-\frac{X^2}{2}\right)dX,$$

which can be calculated with the use of asymptotic equations for "peak," "tail," and "sloping." It is found that $\Upsilon \sim 2.0556$.

This leads to

$$d \sim h + \frac{1}{\sqrt{2\pi}}\frac{\Lambda^{3/2}}{\lambda^{1/2}}\exp\left(-\frac{h}{\lambda}\right) - \Upsilon\frac{4\Lambda^3}{\pi^3\lambda^2}\exp\left(-\frac{2h}{\lambda}\right)$$

$$= h + \frac{1}{\sqrt{2\pi}}\frac{\Lambda^{3/2}}{\lambda^{1/2}}\exp\left(-\frac{h}{\lambda}\right)$$
$$\times \left(1 - \Upsilon\frac{2\sqrt{2}}{\pi^2\sqrt{\pi}}\left(\frac{\Lambda}{\lambda}\right)^{3/2}\exp\left(-\frac{h}{\lambda}\right)\right). \tag{B.1}$$

By construction of the expansion, the ratio of the second order term to the first order one should be small, viz.:

$$\Upsilon\frac{2\sqrt{2}}{\pi^2\sqrt{\pi}}\left(\frac{\Lambda}{\lambda}\right)^{3/2}\exp\left(-\frac{h}{\lambda}\right) \ll 1. \tag{B.2}$$

This quantity is plotted as dashed lines in Fig. 3B. It is observed that the condition (B.2) is satisfied even in the domain where $(d - h)/h$ (represented as solid lines in Fig. 3B) is not necessarily small. This gives an indication that the range of applicability of our first approximation is larger than that anticipated from Fig. 3A.

Note also that using (15), the condition (B.2) may be rewritten as

$$\left|1 - \frac{R}{R_{\text{eff}}}\right| \ll \frac{8\Upsilon}{\pi^2} \sim 1.6662.$$

Physically, this means that the area of applicability of the first order solution can be extended in case the change in curvature is small enough.

## References

[1] J.N. Israelachvili, Intermolecular and Surface Forces, Academic Press, London, 1985.
[2] K.L. Johnson, K. Kendall, A.D. Roberts, Proc. R. Soc. London Ser. A 324 (1971) 301.
[3] B.V. Derjaguin, V.M. Muller, Y.P. Toporov, J. Colloid Interface Sci. 53 (1975) 314.
[4] D. Maugis, J. Colloid Interface Sci. 150 (1992) 243.
[5] J.A. Greenwood, Proc. R. Soc. London Ser. A 453 (1997) 1277.
[6] V.M. Muller, V.S. Yushchenko, B.V. Derjaguin, J. Colloid Interface Sci. 77 (1980) 91.
[7] P. Attard, J.L. Parker, Phys. Rev. A 46 (1992) 7959.
[8] J.Q. Feng, Colloids Surf. A 172 (2000) 175.
[9] B.D. Hughes, L.R. White, Q. J. Mech. Appl. Math. 32 (1979) 445.
[10] B.D. Hughes, L.R. White, J. Chem. Soc. Faraday Trans. 1 76 (1980) 963.
[11] J.L. Parker, P. Attard, J. Phys. Chem. 96 (1992) 10,398.
[12] O.I. Vinogradova, F. Feuillebois, Langmuir 18 (2002) 5126.
[13] B.V. Derjaguin, L.D. Landau, Acta Physicochim. URSS 14 (1941) 633.
[14] E.J.W. Verwey, J.T.G. Overbeek, Theory of the Stability of Lyophobic Colloids, Elsevier, Amsterdam, 1948.
[15] R.M. Pashley, Adv. Colloid Interface Sci. 16 (1982) 57.
[16] P. Claesson, H.K. Christenson, J. Phys. Chem. 92 (1988) 1650.
[17] J.N. Israelachvili, R.M. Pashley, Nature 300 (1982) 341.
[18] P. Kekicheff, O. Spalla, Phys. Rev. Lett. 75 (1995) 1851.
[19] J.N. Israelachvili, G.E. Adams, J. Chem. Soc. Faraday Trans. 1 74 (1978) 975.
[20] W.A. Ducker, T.J. Senden, R.M. Pashley, Nature 353 (1991) 239.
[21] D.Y.C. Chan, R.R. Dagastine, L.R. White, J. Colloid Interface Sci. 236 (2001) 141.
[22] B. Snyder, D. Aston, J. Berg, Langmuir 13 (1997) 590.
[23] V.V. Lulevich, I.L. Radtchenko, G.B. Sukhorukov, O.I. Vinogradova, J. Phys. Chem. B 107 (2003) 2735.
[24] G. Gilles, C.A. Prestiges, P. Attard, Langmuir 17 (2001) 7955.
[25] F.J. Schmitt, T. Ederth, P. Wiedenhammer, P. Claesson, H.J. Jacobasch, J. Adhes. Sci. Technol. 13 (1999) 79.
[26] J.L. Parker, Prog. Surf. Sci. 47 (1994) 205.
[27] B.V. Derjaguin, Kolloid Z. 69 (1934) 155.
[28] L.R. White, J. Colloid Interface Sci. 95 (1983) 286.
[29] O.I. Vinogradova, Langmuir 11 (1995) 2213.
[30] O.I. Vinogradova, Langmuir 12 (1996) 5963.
[31] L.D. Landau, E.M. Lifshitz, Theory of Elasticity, Pergamon, London, 1959.
[32] R.H. Davis, J.-M. Serayssol, E.J. Hinch, J. Fluid Mech. 163 (1986) 479.

[33] O.I. Vinogradova, F. Feuillebois, J. Colloid Interface Sci. 221 (2000) 1.

[34] V.S.J. Craig, B.W. Ninham, R.M. Pashley, Langmuir 14 (1998) 3326.

[35] O.I. Vinogradova, G.E. Yakubov, H.J. Butt, J. Chem. Phys. 114 (2001) 8124.

[36] R.G. Horn, J.N. Israelachvili, F. Pribac, J. Colloid Interface Sci. 115 (1987) 480.

[37] Y.L. Chen, C.A. Helm, J.N. Israelachvili, J. Phys. Chem. 95 (1991) 10,736.

[38] H.K. Christenson, Langmuir 12 (1996) 1404.

[39] J.N. Connor, R.G. Horn, Langmuir 17 (2001) 7194.

[40] O.I. Vinogradova, Langmuir 14 (1998) 2827.

[41] O.I. Vinogradova, H.-J. Butt, G.E. Yakubov, F. Feuillebois, Rev. Sci. Instrum. 72 (2001) 2330.

[42] S.J. Miklavcic, R.G. Horn, D.J. Bachmann, J. Phys. Chem. 99 (1995) 16,357.

[43] S.J. Miklavcic, Phys. Rev. E 57 (1998) 561.

[44] O.I. Vinogradova, R.G. Horn, Langmuir 17 (2001) 1604.

[45] J.B. Pethica, A.P. Sutton, J. Vac. Sci. Technol. A 6 (1988) 2490.

[46] J.R. Smith, G. Bozzolo, A. Banerjea, J. Ferrante, Phys. Rev. Lett. 63 (1989) 1269.